REPORT DOCUMENTATION PAGE

Form Approved
OMB No. 0704-0188

PLEASE DO NOT RETURN YOUR FORM TO THE ABOVE ADDRESS.

1. REPORT DATE *(DD-MM-YYYY)*	2. REPORT TYPE	3. DATES COVERED *(From - To)*
01-04-2009	Journal Article	March 2007 - March 2008

4. TITLE AND SUBTITLE

DOA estimation and multi-user interference in a two-radar system

5a. CONTRACT NUMBER

N/A

5b. GRANT NUMBER

N/A

5c. PROGRAM ELEMENT NUMBER

612311

6. AUTHOR(S)

Maria Greco*, Fulvio Gini*, Alfonso Farina**, and Muralidhar Rangaswamy

5d. PROJECT NUMBER

2311

5e. TASK NUMBER

HE

5f. WORK UNIT NUMBER

02

7. PERFORMING ORGANIZATION NAME(S) AND ADDRESS(ES)

Electromagnetic Scattering Branch
Air Force Research Laboratory, Sensors Directorate
80 Scott Drive
Hanscom AFB, MA 01731-2909

*Univ. of Pisa, Italy
** Selex-Sistemi Integrati
Rome, Italy

8. PERFORMING ORGANIZATION REPORT NUMBER

N/A

9. SPONSORING/MONITORING AGENCY NAME(S) AND ADDRESS(ES)

Electromagnetics Technology Division SC: 437490
Sensors Directorate
Air Force Research Laboratory
80 Scott Drive Hanscom AFB, MA 01731-2909

10. SPONSOR/MONITOR'S ACRONYM(S)

AFRL-RY-HS

11. SPONSOR/MONITOR'S REPORT NUMBER(S)

AFRL-RY-HS-TP-2009-0006

12. DISTRIBUTION/AVAILABILITY STATEMENT

Distribution A: Approved for UNLIMITED DISTRIBUTION

13. SUPPLEMENTARY NOTES

Research support by Air Force Office of Scientific Research. Cleared for public release approved by 88 ABW/PA Public Affairs Office, WPAFB, OH: RY-08-0423

14. ABSTRACT

In this paper,we investigate the impact of the presence of interfering radar on the target direction of arrival (DOA) estimation performed by the reference radar.The analyzed estimators are the pseudo-monopulse and the maximum likelihood techniques.The importance of the use of codes in multi-user radar system is highlighted in a simple scenario of two radars by calculating the root-mean square error of the estimators in different operational conditions and comparing them with the Cramer-Rao lower bounds.

15. SUBJECT TERMS

Frequency-hop-coded signals, auto and cross-ambiguity function, monopulse radar, DOA estimation, maximum likelihood, Cramer-Rao lower bounds, radar networks

16. SECURITY CLASSIFICATION OF:			17. LIMITATION OF ABSTRACT	18. NUMBER OF PAGES	19a. NAME OF RESPONSIBLE PERSON
a. REPORT	b. ABSTRACT	c. THIS PAGE			Muralidhar Rangaswamy
U	U	U	UU	11	19b. TELEPHONE NUMBER *(Include area code)* 781-377-3446

Reset

Standard Form 298 (Rev. 8/98)
Prescribed by ANSI Std. Z39.18

Signal Processing 89 (2009) 355–364

Contents lists available at ScienceDirect

Signal Processing

journal homepage: www.elsevier.com/locate/sigpro

DOA estimation and multi-user interference in a two-radar system ☆

Maria Greco [a,*], Fulvio Gini [a], Alfonso Farina [b,1], Muralidhar Rangaswamy [c,2]

[a] Dip. di Ingegneria dell'Informazione, University of Pisa, via G. Caruso, 14-56122 Pisa, Italy
[b] SELEX-Sistemi Integrati, via Tiburtina Km. 12.400–00131 Rome, Italy
[c] Air Force Research Laboratory Sensors Directorate, 80 Scott Dr. Hanscom Air Force Base, MA 01731-2909, USA

ARTICLE INFO

Article history:
Received 3 August 2007
Received in revised form
22 May 2008
Accepted 29 August 2008
Available online 23 September 2008

Keywords:
Frequency hop-coded signals
Auto and cross-ambiguity function
Monopulse radar
DOA estimation
Maximum likelihood
Cramér-Rao lower bounds
Radar network

ABSTRACT

In this paper, we investigate the impact of the presence of interfering radar on the target direction of arrival (DOA) estimation performed by the reference radar. The analyzed estimators are the pseudo-monopulse and the maximum likelihood techniques. The importance of the use of codes in multi-user radar system is highlighted in a simple scenario of two radars by calculating the root-mean square error of the estimators in different operational conditions and comparing them with the Cramér-Rao lower bounds.

1. Introduction

For many years, conventional radars transmitted, received, and processed the same waveform on every pulse or burst within a coherent processing interval, independently of the environment. In the 1970s, adaptive processing began to be developed. For the first time, the processing of received signals changed depending on the environment (noise, clutter, and interferences). Radars began to be more flexible on receive.

Now, modern radar systems have considerable flexibility in their modes of operation, both on receive and transmit. In particular, it is possible to modify the waveform on a pulse-to-pulse basis, and electronically steered phased arrays can quickly point the radar beam in any feasible direction. Such flexibility calls for new methods of designing and scheduling the waveforms to optimize the radar performance. Then, an agile and diverse waveform radar system should be able to change on the fly the transmitted waveform based on the information estimated or a priori known on the environment, on the targets and the jammers [1].

Moreover, in a radar network each sensor should also be able to operate and perform its task without negatively interfering with the other sensors and, possibly, to improve the performance of the whole network. Then, the waveforms used by the radars in a complex network should be designed and changed on the fly, based on the clutter, target and interference echoes[3]; they should guarantee good target detection and parameter estimation

☆ This work has been partially funded by AFOSR grant FA8655-07-1-3096. The views and conclusions contained herein are those of the authors and should not be interpreted as necessarily representing the official policies or endorsements, either expressed or implied, of the Air Force Office of Scientific Research or the U.S. Government.

* Corresponding author. Tel.: +39 050 2217620; fax: +39 050 2217522.
E-mail addresses: m.greco@ing.unipi.it (M. Greco), f.gini@ing.unipi.it (F. Gini), afarina@selex-si.com (A. Farina), Muralidhar.Rangaswamy@hanscom.af.mil (M. Rangaswamy).
[1] Tel.: +39 06 4150 2279; fax: +39 06 4150 3755.
[2] Tel.: +1 781 3773446; fax: +1 781 3778984.

0165-1684/$ - see front matter © 2008 Elsevier B.V. All rights reserved.
doi:10.1016/j.sigpro.2008.08.013

[3] The choice of the transmitted waveform depends not only on the desired delay and Doppler resolution, but also on where the clutter or competing targets are located in the delay-Doppler plane [5].

in different scenarios and should allow an optimal access to the same transmit channel.

To perform good target detection and estimation, frequency hop pulse train signals are often used in high resolution radar systems. These signals are characterized by an auto-ambiguity function (AAF) that exhibits a narrow thumb tack shape with low sidelobes. In contrast, in application like multi-access communications, attention is paid in designing a sequence of frequency-hopped coded waveforms with small cross-correlation functions. In multi-user radar system scenarios both objectives are desirable. Unfortunately, there is a tradeoff between these objectives. Frequency hop pulse trains based on Costas codes, for instance, are known to have almost ideal AAF but not very good cross-ambiguity properties [2]. On the contrary, frequency-coded signals based on linear congruences [3] have ideal cross- but unattractive auto-ambiguity properties. Some attempt to design multiple access frequency hop codes with good cross-ambiguity function (CAF) has been done, for instance, in [4] where the frequency hop patterns were constructed upon an extension of the theory of quadratic congruences.

The scenario analyzed in this paper is composed of two radars transmitting in the same band, which can illuminate the same area looking for the same target; they can use either the same or different codes. We rewrite the observed signal as a function of cross- and auto-ambiguity function values and target parameters, and we investigate the impact of the presence of the transmitted signal of the second radar (the interfering radar) on the first one (the reference radar) in the estimation of the target direction of arrival (DOA). We analyzed two DOA estimators, the pseudo-monopulse (PM) and the maximum likelihood (ML) estimator and we compared their performances with the Cramèr-Rao lower bounds (CRLB). We focused our attention only on the influence of the interfering radar on the DOA estimation, so in our scenario we did not simulate jammers or correlated clutter.

The paper is organized as follows. In Section 2, the received signal model is explained and the PM and the ML techniques for DOA estimation are summarized. In Section 3, the results of the analysis are described. In Section 4, the CRLB for the problem at hand is derived and compared with the root-mean square error (RMSE) of the PM and ML estimators. In Section 5, some conclusions on the use of codes are drawn.

2. Problem statement

The scenario is pictorially drawn in Fig. 1. Two radars scan the same area transmitting frequency-coded bursts of pulses and listening to the echo of a possible target. The complex envelope of the transmitted unitary power signal is given by

$$u(t) = \frac{1}{\sqrt{M\tau_c}} \sum_{m=1}^{M} u_m(t-(m-1)\tau_c), \tag{1}$$

where

$$u_m(t) = \begin{cases} \exp(j2\pi f_m t) & 0 \leqslant t \leqslant \tau_c, \\ 0 & \text{elsewhere}, \end{cases} \tag{2}$$

M is the number of subpulses for each transmitted pulse of time duration T_i, $\tau_c = T_i/M$ is the duration of each subpulse and $\{f_m\}_{m=1}^{M}$ is the sequence of frequencies related to the code used by the radar. For Costas arrays, for instance, $f_m = d_m/\tau_c$, where d_m belongs to the sequence $\mathbf{d}_M = \{d_0, d_1, \ldots, d_m, \ldots, d_{M-1}\}$, which is a permutation of the

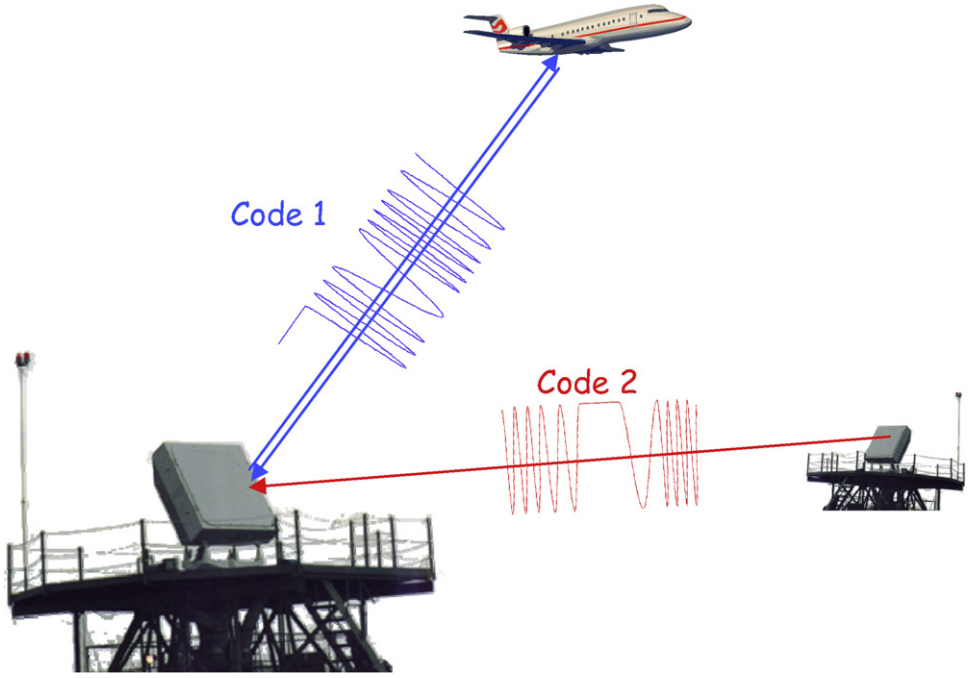

Fig. 1. Radar scenario.

integer numbers $J_M = \{0,1,\ldots,M-1\}$. The choice of $\{f_m\}_{m=1}^{M}$, characterizing the frequency code is critical and of paramount importance in defining the properties of the auto- and cross-ambiguity functions of the transmitted signal. A detailed description of this topic can be found in [5].

As known, the AAF represents the time response of a filter matched to a given finite energy signal when the signal is received with a delay τ and a Doppler shift v relative to the nominal zeros values expected by the filter [5]. Then, the AAF definition is

$$|\mathrm{A}(\tau,v)| = \left| \int_{-\infty}^{+\infty} u(t)u^*(t+\tau)\exp(\mathrm{j}2\pi v t)\mathrm{d}t \right|, \tag{3}$$

where $u(t)$ is the complex envelope of the signal. The CAF between two signals $u_1(t)$ and $u_2(t)$ is similarly defined as[4]

$$|C(\tau,v)| = \left| \int_{-\infty}^{+\infty} u_1(t)u_2^*(t+\tau)\exp(\mathrm{j}2\pi v t)\mathrm{d}t \right|. \tag{4}$$

2.1. Signal model

In the reference radar, the received signal is first down-shifted to an intermediate frequency IF and amplified. The IF signal is then processed as in the scheme of Fig. 2, where LO is a local oscillator tuned on the IF frequency, LPF is a low pass filter and A/D is an analog-to-digital device.

Before the digitalization, the inphase (I) and (Q) quadrature components of the target signal are:

$$x_{\mathrm{I}}(t) = a\cos\left(2\pi\frac{\mathrm{d}(t)}{\tau_{\mathrm{c}}}t + 2\pi f_{\mathrm{D}}t - \varphi\right), \tag{5}$$

$$x_{\mathrm{Q}}(t) = a\sin\left(2\pi\frac{d(t)}{\tau_{\mathrm{c}}}t + 2\pi f_{\mathrm{D}}t - \varphi\right), \tag{6}$$

where $a\exp(\mathrm{j}\varphi)$ is the complex amplitude of the target that depends on the radar-cross section (RCS) and on the antenna gain, f_{D} is the Doppler frequency, and $\mathrm{d}(t) = \sum_{m=0}^{M-1} d_m \cdot \mathrm{rect}((t-m\tau_{\mathrm{c}}/2)\tau_{\mathrm{c}})$ is the frequency code.

After the digitalization at a sampling frequency f_{c}, the complex envelope of the received target signal is given by

$$x(n/f_{\mathrm{c}}) = a\mathrm{e}^{\mathrm{j}\varphi}\exp\left(2\pi\frac{\mathrm{d}(n/f_{\mathrm{c}})}{\tau_{\mathrm{c}}f_{\mathrm{c}}}n + 2\pi\frac{f_{\mathrm{D}}}{f_{\mathrm{c}}}n\right). \tag{7}$$

In the correlator of Fig. 2, the sequence of $x(n/f_{\mathrm{c}})$ is correlated with the sequence of samples of the transmitted signal. Then the output signal is given by[5]

$$x = a\mathrm{e}^{\mathrm{j}\varphi}\sum_{n=0}^{N_{\mathrm{S}}-1} u(n/f_c)x^*(n/f_c) = a\mathrm{e}^{\mathrm{j}\varphi}A. \tag{8}$$

It is easy to compare the term A in Eq. (8) with Eqs. (3) and (4). If N_{S} is large we can consider the sum as a good approximation of the integral. Moreover, if the received signal $x(n/f_{\mathrm{c}})$ is a delayed and frequency shifted copy of the transmitted signal $u(n/f_{\mathrm{c}})$, we can state that A is the value of the complex AAF of the signal for some delay τ and Doppler target shift f_{D}; then $A = A(\tau f_{\mathrm{D}})$. This is the case of the signal backscattered by a target illuminated by the reference radar. If, on the contrary, the signal received by the reference radar is the signal transmitted by the interfering radar, A is the value of the complex CAF; that is $A = C(\tau_{\mathrm{R}}, f_{\mathrm{D_R}})$. If both signals are present, the received signal is given by

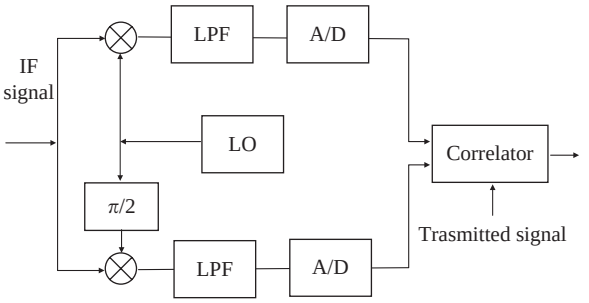

Fig. 2. Receiver scheme.

$$y = a\mathrm{e}^{\mathrm{j}\varphi}A(\tau,f_{\mathrm{D}}) + b\mathrm{e}^{\mathrm{j}\theta}C(\tau_{\mathrm{R}},f_{\mathrm{D_R}}) + d, \tag{9}$$

where $b\mathrm{e}^{\mathrm{j}\theta}$ is the complex amplitude of the signal relating to the second radar and d is the unavoidable contribution of the disturbance (thermal noise plus clutter).

2.2. Pseudo-monopulse estimator

In the analyzed scenario the reference radar is supposed to estimate the DOA of the target by using a pseudo-monopulse technique or the maximum likelihood estimator [6].

In a typical phased array radar, a single beam is formed on transmission and two or more beams are formed on reception. We assume here that the system is a linear array radar that estimates the target DOA by using the sum channel $\sum$ on transmission and two matched channels, the sum $\sum$ and the difference Δ on reception. The two channels, or antenna patterns, are defined as the complex amplitude profiles versus target azimuth angle θ_{T}. The sum channel pattern is denoted by $f_{\sum}(\theta)$ and the difference pattern by $f_{\Delta}(\theta)$; these patterns are chosen here as in [6], the -3 dB beamwidth is $\theta_{\mathrm{B}} = 3^{\circ}$. The PM technique used here is very similar to the classical monopulse method, based on the ratio of the Δ and $\sum$ channel outputs y_{Δ} and $y_{\sum}$. It uses N pulses transmitted by the radar in the time-on-target (ToT), while the antenna beams are electronically or mechanically steered with constant angular velocity ω_{R} rad/s. The number N of pulses between the one-way -3 dB points is given by $N = \theta_{\mathrm{B}}/(\omega_{\mathrm{R}}T)$, where $T = 1/\mathrm{PRF}$ is the radar pulse repetition time and PRF is the corresponding pulse repetition frequency. The antenna introduces an amplitude modulation on the target signal, in both the channels, that depends on the target azimuth position and on the instantaneous boresight of the array.

Based on Eq. (9), it is possible to write the expression of the signal received on the sum and on the difference

[4] The calculation of Eqs. (4) and (5) is not always easy. For some frequency code it is useful to resort to the placement and difference matrices, as explained in [3,14].

[5] We did not use any window in the calculation of Eq. (8).

channels. Let us suppose that the Doppler frequencies of the target and of the interference radar are the same with respect to the reference radar. In this case, the reference radar cannot distinguish between the two signals by means of Doppler processing. Without lack of generality, we assume that both Doppler frequencies are null; then the received signals are given by

$$y_\Sigma(n) = \alpha A f_\Sigma^2(\theta_T, n) + \beta C f_\Sigma(\theta_I, n) + d_\Sigma(n), \tag{10a}$$

$$y_\Delta(n) = \alpha A f_\Sigma(\theta_T, n) f_\Delta(\theta_T, n) + \beta C f_\Delta(\theta_I, n) + d_\Delta(n), \tag{10b}$$

where $n = 0,1,\ldots,N-1$. With respect to Eq. (9), the dependence of the complex amplitudes of target and interfering signal on the antenna patterns has been explicitly indicated. The first term in y_Σ and y_Δ is due to the target signal; it depends on the target DOA θ_T through $f_\Sigma^2(\theta_T)$ in sum channel and through $f_\Sigma(\theta_T)f_\Delta(\theta_T)$ in the difference channel. This is due to the two-way antenna gain. The second term is due to the signal transmitted by the second radar which has a DOA θ_I and it depends on the one-way gain of the antenna pattern ($f_\Sigma(\theta_I)$ and $f_\Delta(\theta_I)$). d_Σ and d_Δ are the noises on the two channels.

The signal processor forms the monopulse ratio defined by $r(n) = \mathrm{Re}\{y_\Delta(n)/y_\Sigma(n)\}$ for each pulse where Re{} denotes the real part. In absence of disturbance and in the presence of only one target, the monopulse ratio reduces to $r(n) = \mathrm{Re}\{f_\Delta(\theta_T,n)/f_\Sigma(\theta_T,n)\}$ from which the angular location of the target for each pulse can be determined. Finally, we obtain $\hat{\theta}_{TG} = \sum_{n=0}^{N-1}\hat{\theta}_{TG}^{(n)}/N$, where $\hat{\theta}_{TG}^{(n)}$ is the target DOA estimate for each pulse.

We treat the situation in which the source can be considered static with respect to the radar during the ToT, that is, during the recording of the N pulses. In this case, due to the scanning movement of the antenna only, the proposed estimator is biased and the bias can be calculated. It is easy to verify that $b = E\{\hat{\theta}_{TG} - \theta_{TG}\} = (N-1)\theta_B/(2N)$ then a DOA unbiased estimator is $\hat{\theta}_{TG} = \sum_{n=0}^{N-1}\hat{\theta}_{TG}^{(n)}/N - b$ [6].

2.3. Maximum likelihood estimator

If we rewrite Eq. (10) in vector notation, the data model is given by $\mathbf{y} = \alpha_T\mathbf{g}(\theta_T)+\alpha_I\mathbf{f}(\theta_I)+\mathbf{d}$, where $\alpha_T = \alpha A$, and $\alpha_I = \beta C$, $\mathbf{g}(\theta_T) = [\mathbf{g}_\Sigma^T\mathbf{g}_\Delta^T]^T$ is the $2N\times 1$ steering vector of the target, $[\mathbf{g}_\Sigma]_n = f_\Sigma^2(\theta_T,n)$ and $[\mathbf{g}_\Delta]_n = f_\Sigma(\theta_T,n)f_\Delta(\theta_T,n)$. $\mathbf{f}(\theta_T) = [\mathbf{f}_\Sigma^T\mathbf{f}_\Delta^T]^T$ is the steering vector of the interference, with $[\mathbf{f}_\Sigma]_n = f_\Sigma(\theta_T,n)$ and $[\mathbf{f}_\Delta]_n = f_\Delta(\theta_T,n)$. The $2N\times 1$ disturbance vector $\mathbf{d}$ is given by $\mathbf{d} = [\mathbf{d}_\Sigma^T\mathbf{d}_\Delta^T]^T$. The ML estimator of θ_T,[6] when the observed vector does not contain the interference and the vector $\mathbf{d}$ is modeled as a complex Gaussian vector with a covariance matrix $\mathbf{M}$, is given by

$$\hat{\theta}_{ML} = \underset{\theta}{arg\max}\frac{|\mathbf{y}^H\mathbf{M}^{-1}\mathbf{g}(\theta)|^2}{\mathbf{g}^H(\theta)\mathbf{M}^{-1}\mathbf{g}(\theta)}. \tag{11}$$

In the next paragraph we investigate the impact of the presence of the interfering radar on the DOA RMSE when the estimation is performed by the PM and the ML techniques.

3. Simulation results

To evaluate the impact of the presence of the interfering radar, the RMSE, the variance and the bias of the DOA estimator has been derived by running 10^4 Monte Carlo simulations. The disturbance is modeled as a complex white Gaussian process, in short notation $\mathbf{d}\sim\mathrm{CN}(\mathbf{0},\sigma_d^2\mathbf{I})$, where $\mathbf{I}$ the $2N$-dimensional identity matrix, the target and interference signal amplitudes α_T and α_I are modeled first as: (i) complex Gaussian independent random variables, in short $\alpha_T\sim\mathrm{CN}(0,\sigma_T^2|A|^2)$ and $\alpha_I\sim\mathrm{CN}(0,\sigma_I^2|C|^2)$; and then as: (ii) deterministic unknown parameters. In the first case, the signal-to-noise (SNR) power ratio is defined as $\mathrm{SNR} = |A|^2\cdot\sigma_T^2/\sigma_d^2$ and the signal-to-interference ratio as $\mathrm{SIR} = \sigma_T^2/\sigma_I^2$; in the second case, $\mathrm{SNR} = |\alpha_T|^2\cdot/\sigma_d^2$ and $\mathrm{SIR} = |\alpha_T/\alpha_I|^2$.

The results of our analysis are shown in Figs. 3–7 for the PM estimator and in Figs. 8–14 for the ML estimator. We set $\mathrm{SNR} = 20\,\mathrm{dB}$,[7] $\mathrm{SIR} = 0\,\mathrm{dB}$ and $N = 16$; the target DOA has been set equal to 1.5° ($\theta_T = 1.5^\circ$). We investigated also other target DOA positions in the main beam of the antenna. The behavior of the estimators is similar, and then we show here the results for one position only.

Due to the high value of SNR, the performance of the PM and ML estimators are mainly affected by the presence of the interfering radar; they are the functions of the ratio $|C/A|$. The value of C and A depends on the code used by both radars and on the synchronization between transmit and receive of the reference radar and between reference and interfering radar.

If the reference radar is synchronized in reception and transmission and the receiver is tuned on the Doppler of the target, $\tau = 0$ and $f_D = 0$, then A is the energy of the transmitted pulse. In our analysis we considered $A = 1$ (unit energy pulse) and $0\leqslant|C/A|\leqslant 1$. The worst case is when $|C/A| = 1$; this value characterizes two synchronized radars using the same code. The best case is when $|C/A| = 0$; this value characterizes the case of synchronized radars using two orthogonal codes.

In Fig. 3, we report the RMSE(θ_T) of the PM estimator as a function of the interference DOA, with $\alpha_T\sim\mathrm{CN}(0,\sigma_T^2|A|^2)$ and $\alpha_I\sim\mathrm{CN}(0,\sigma_I^2|C|^2)$. In Fig. 4, we report the bias of the PM estimator in the same scenario. The bias of the estimator increases with $|C/A|$ and the RMSE gets values close to the 40% of the beamwidth. The behavior of both RMSE and bias are almost symmetric with respect to the position of the target θ_T. When $\theta_I = \theta_T$, the bias due to the presence of

[6] As shown in [6], Eq. (11) represents the ML estimator of θ_T when the amplitude α_T is modeled as a deterministic unknown value. When α_T is a random variable, the ML estimator has not a closed form. We adopt here the ML estimator for deterministic α_T even if in our data model the complex amplitude is random; with an abuse of terminology we continue to refer to (11) as the ML estimator.

[7] With this value of SNR the probability of detection of the filter matched to the transmitted signal is almost unitary, even for $P_{FA} = 10^{-6}$.

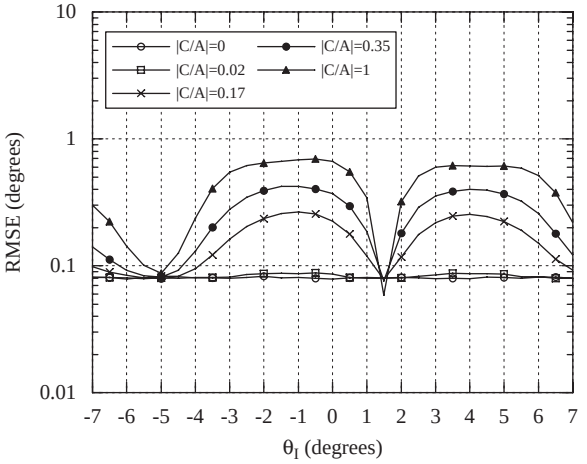

Fig. 3. RMSE vs. interference DOA, $\theta_T = 1.5^\circ$, SNR = 20 dB, SIR = 0 dB, $N = 16$, random α and β, PM estimator.

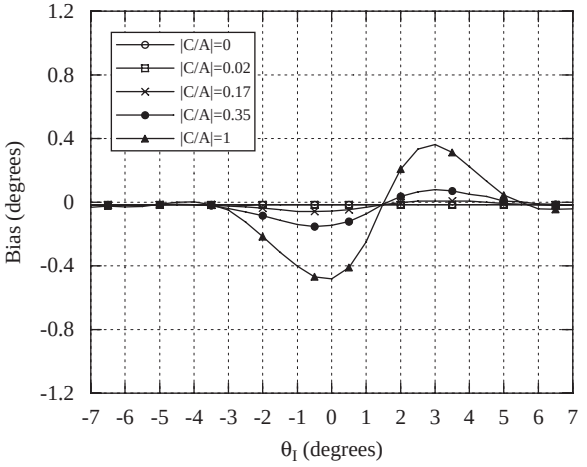

Fig. 4. Bias vs. interference DOA, $\theta_T = 1.5^\circ$, SNR = 20 dB, SIR = 0 dB, $N = 16$, random α and β, PM estimator.

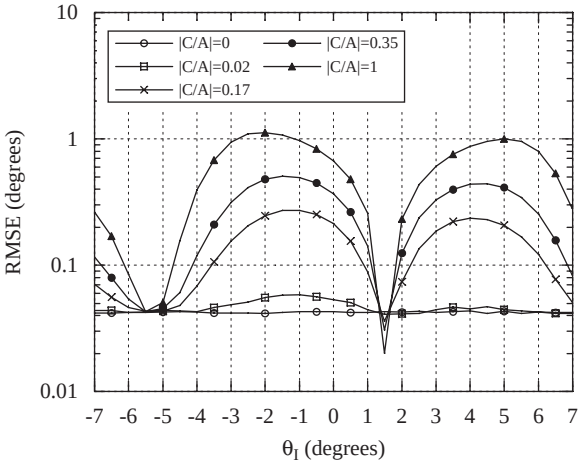

Fig. 5. RMSE vs. interference DOA, $\theta_T = 1.5^\circ$, SNR = 20 dB, SIR = 0 dB, $N = 16$, deterministic α and β, PM estimator.

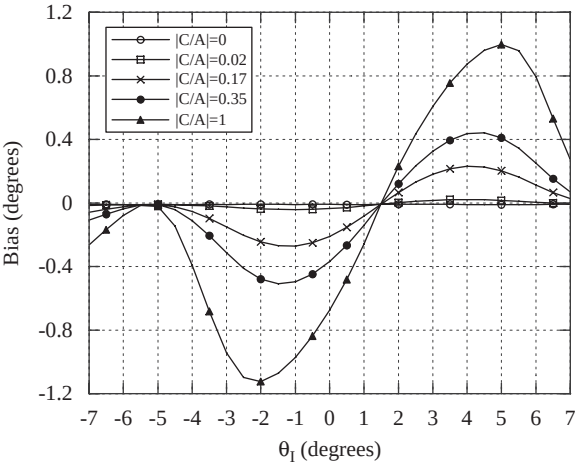

Fig. 6. Bias vs. interference DOA, $\theta_T = 1.5^\circ$, SNR = 20 dB, SIR = 0 dB, $N = 16$, deterministic α and β, PM estimator.

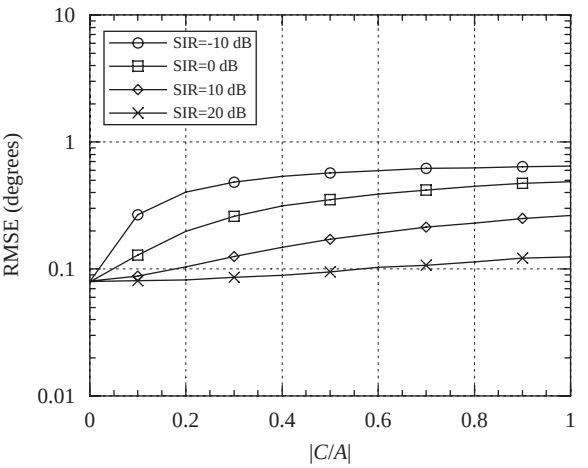

Fig. 7. RMSE vs. $|C/A|$, $\theta_T = 1.5^\circ$, SNR = 20 dB, $N = 16$, $\theta_I \in U(-7^\circ, 7^\circ)$, random α and β, PM estimator.

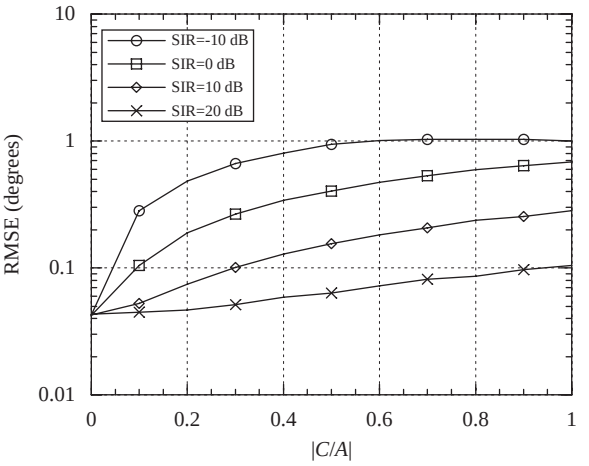

Fig. 8. RMSE vs. $|C/A|$, $\theta_T = 1.5^\circ$, SNR = 20 dB, $N = 16$, $\theta_I \in U(-7^\circ, 7^\circ)$, deterministic α and β, PM estimator.

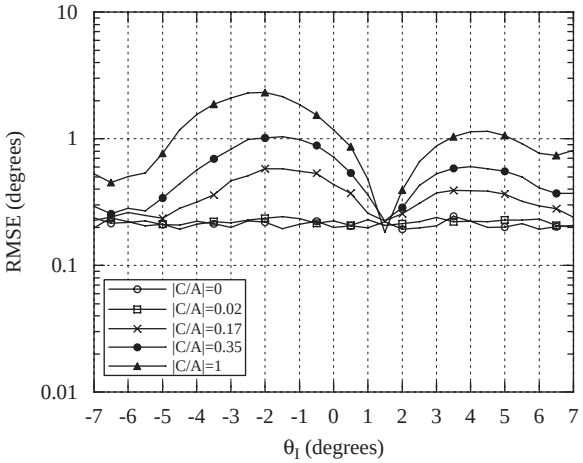

Fig. 9. RMSE vs. interference DOA, $\theta_T = 1.5^\circ$, SNR = 20 dB, SIR = 0 dB, $N = 16$, random α and β, ML estimator.

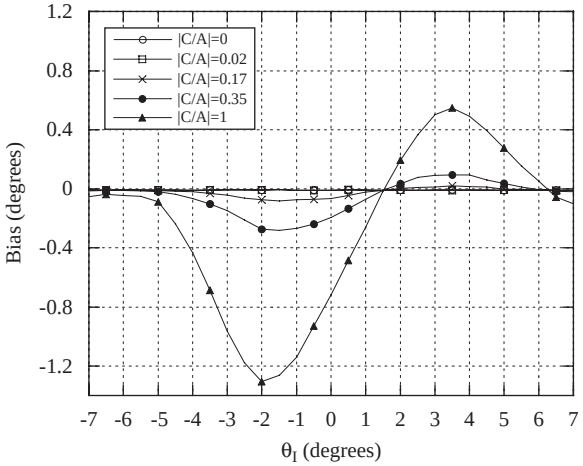

Fig. 10. Bias vs. interference DOA, $\theta_T = 1.5^\circ$, SNR = 20 dB, SIR = 0 dB, $N = 16$, random α and β, ML estimator.

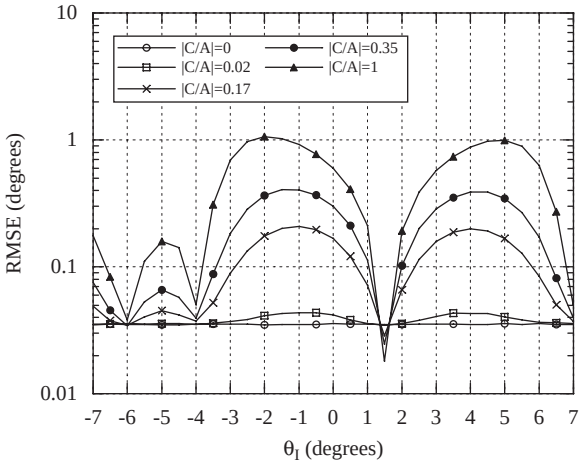

Fig. 11. RMSE vs. interference DOA, $\theta_T = 1.5^\circ$, SNR = 20 dB, SIR = 0 dB, $N = 16$, deterministic α and β, ML estimator.

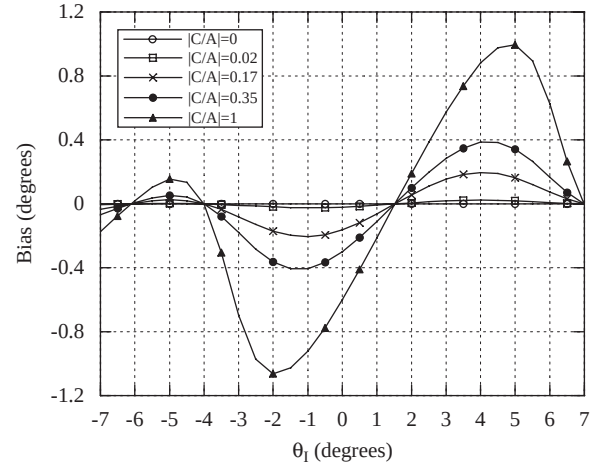

Fig. 12. Bias vs. interference DOA, $\theta_T = 1.5^\circ$, SNR = 20 dB, SIR = 0 dB, $N = 16$, deterministic α and β, ML estimator.

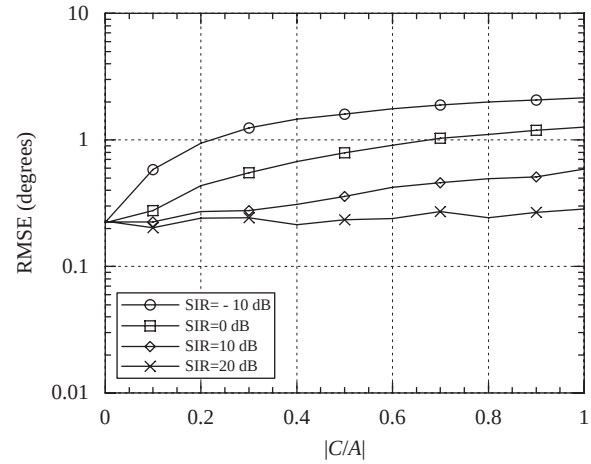

Fig. 13. RMSE vs. $|C/A|$, $\theta_T = 1.5^\circ$, SNR = 20 dB, $N = 16$, $\theta_I \in U(-7^\circ, 7^\circ)$, random α and β, ML estimator.

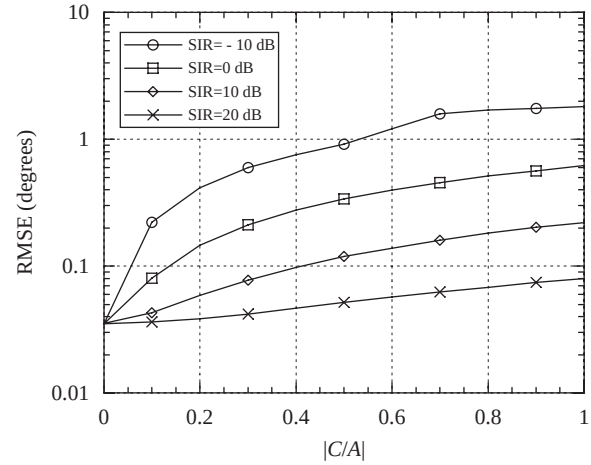

Fig. 14. RMSE vs. $|C/A|$, $\theta_T = 1.5^\circ$, SNR = 20 dB, $N = 16$, $\theta_I \in U(-7^\circ, 7^\circ)$, deterministic α and β, ML estimator.

the interfering radar is null and the RMSE($\hat{\theta}_T$) for $|C/A| = 1$ is lower than that for $|C/A| = 0$.

Similar remarks can be drawn from Figs. 5 and 6, where we report RMSE($\hat{\theta}_T$) and bias for deterministic unknown α_T and α_I. For small $|C/A|$, the RMSE($\hat{\theta}_T$) of the PM estimator is lower when the target and interference amplitudes are deterministic than when they are complex Gaussian random variables. Conversely, the RMSE($\hat{\theta}_T$) is more sensitive to high values of $|C/A| = 0$ when the amplitudes are deterministic than when they are random.

In Figs. 7 and 8, RMSE($\hat{\theta}_T$) is shown as a function of the ratio $|C/A|$ for different value of the SIR, in the case of random and deterministic amplitudes, respectively. The interference DOA θ_I has been generated as a random variable uniformly distributed on the range $[-7^\circ,-7^\circ]$.[8] The impact of the interference is apparent in both figures.

Figs. 9–14 report the companion results for the ML estimator. The behavior is very similar. In the case of deterministic amplitudes the ML estimator outperforms the PM estimator; the contrary in the random amplitude scenario. It is worth reminding that in the case of random amplitude, what in this paper is termed "ML estimator" is not the true ML estimator (for details see [7]).

4. Cramér-Rao lower bounds and performance comparison

To complete our analysis we derived also the CRLB for the two cases at hand. In this section we report results and comments. Detailed derivation of the bounds is presented in Appendices A and B.

When the observed vector $\mathbf{y}$ is complex Gaussian distributed with mean value $\boldsymbol{\mu}_y$ and covariance matrix $\mathbf{C}_y$, in short $\mathbf{y}\sim\mathrm{CN}(\boldsymbol{\mu}_y,\mathbf{C}_y)$, with unknown real parameters $\boldsymbol{\chi} = [\chi_1,\chi_2,\ldots\chi_n]^T$, the elements of the Fisher matrix are given by [8]

$$[\mathbf{J}(\boldsymbol{\chi})]_{i,j} = \mathrm{Tr}\left\{\mathbf{C}_y^{-1}(\chi)\frac{\partial\mathbf{C}_y(\boldsymbol{\chi})}{\partial\chi_i}\mathbf{C}_y^{-1}(\boldsymbol{\chi})\frac{\partial\mathbf{C}_y(\chi)}{\partial\chi_j}\right\} + 2\Re\mathrm{e}\left\{\frac{\partial\boldsymbol{\mu}_y^H(\boldsymbol{\chi})}{\partial\chi_i}\mathbf{C}_y^{-1}(\boldsymbol{\chi})\frac{\partial\boldsymbol{\mu}_y(\boldsymbol{\chi})}{\partial\chi_j}\right\}, \quad (12)$$

where $\mathrm{Tr}\{\cdot\}$ is the trace of a matrix, $\Re\mathrm{e}\{\cdot\}$ stands for the real part and $i,j = 1,2,\ldots,n$.

4.1. Deterministic amplitudes

In this case $\mathbf{C}_y = \sigma_d^2\mathbf{I}$ and $\boldsymbol{\mu}_y = \alpha A\cdot\mathbf{g}(\theta_T)+\beta C\cdot\mathbf{h}(\theta_I)$. Decomposing the complex amplitudes α and β in their modulus an phase, that is $\alpha = ae^{j\varphi}$ and $\beta = be^{j\psi}$, the vector of the real parameters to estimate is $\boldsymbol{\chi} = [\theta_T\ a\ \varphi\ \theta_I\ b\ \psi]^T$. The 36 elements of the Fisher matrix are reported in Appendix A.

As verified in Eq. (A.28), the CRLB of the target parameters θ_T, a, and φ do not depend on the ratio $|C/A|$. This means that, theoretically, if the radar knows that an interference is present, it is possible to find an efficient unbiased estimator that is not sensitive to the code used by both reference and interfering radars. Unfortunately, this never happens. In the existing systems, the radar simply applies some techniques for the estimation of target DOA even when there is an interference, then the presence of an interfering radar biases the estimates increasing the root mean square error more than one order of magnitude with respect to the CRLB, as shown in Fig. 15. In Fig. 15, we report the square root of the Cramér-Rao lower bound (RCRLB) of θ_T in degrees, $\mathrm{RCRLB}(\theta_T) = (180^\circ/\pi)\sqrt{\mathrm{CRLB}(\theta_T)}$, compared to the RMSE($\theta_T$) of ML and PM estimators for $|C/A| = 0$ and $|C/A| = 1$, as a function of the interference DOA. The solid line with white squares (labelled RCRLB) represents the RCRLB(θ_T) calculated when all the target and interference parameters are deterministic and unknown. The dotted

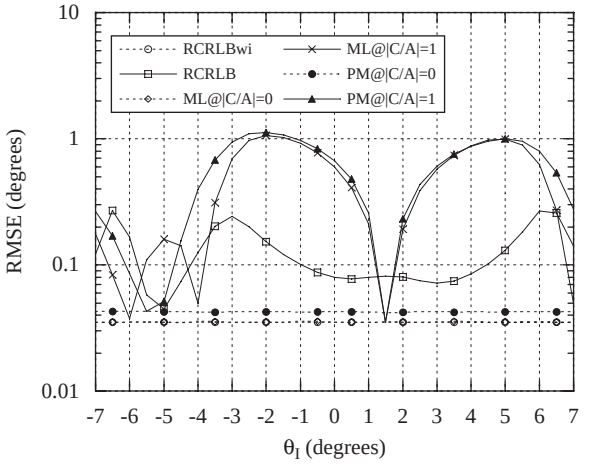

Fig. 15. RMSE of ML and PM estimators and RCRLB vs. interference DOA, $\theta_T = 1.5^\circ$, deterministic α and β.

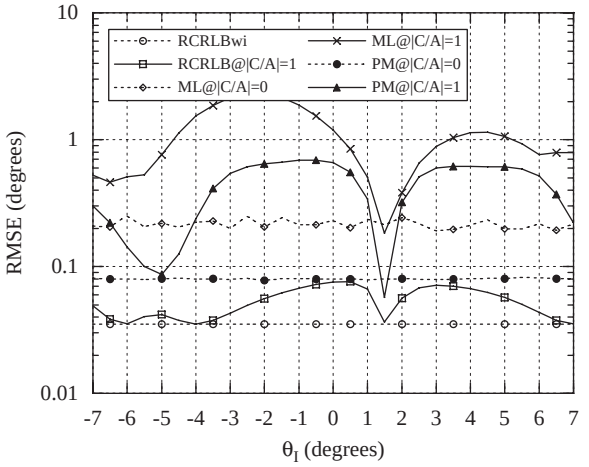

Fig. 16. RMSE of ML and PM estimators and RCRLB vs. interference DOA, $\theta_T = 1.5^\circ$, random α and β.

[8] These are the angular positions of the nulls of first right and left sidelobes of the sum channel.

line with white circles (labelled RCRLBwi) reports the RCRLB(θ_T) calculated when the interference is not present (Eq. (A.29)). It should not seem to be an absurd that for some values of θ_I, the RMSE(θ_T) is smaller than the RCRLB(θ_T), because both ML and PM estimators are biased.

4.2. Random amplitudes

The comparisons in the case of complex Gaussian distributed amplitudes are summarized in Fig. 16. Again, the solid line with white squares (labelled RCRLB@$|C/A|=1$) represents the RCRLB(θ_T) calculated when both target and interference DOAs are unknown and $|C/A|=1$. The dotted line with white circles (labelled RCRLBwi) reports the RCRLB(θ_T) calculated when the interference is not present (Eq. (B.3)). The two curves are close, meaning that also in this case, knowing the presence of the interference, it could be possible to find an estimator that is not too sensitive to the values of $|C/A|$. Unfortunately, also in the case of random amplitude, the performance of realistic estimators as the PM and ML are far from the CRLB and the impact of the codes is heavy.

5. Conclusions

The aim of this paper is to highlight that the proper use of codes is of paramount importance even in a very simple radar network formed by two radars. The impact of the presence of a radar on the other has been measured in the estimation of the target DOA performed by the reference radar. We considered only two multi-pulses algorithms, the ML and the PM, among all the DOA estimation techniques (see for instance [9–12], and references therein) not with the purpose of finding the best algorithm in the presence of an interference, but simply willing to show that two very different techniques suffer the same performance impoverishment. We verified that the interference mainly introduces a bias in the DOA estimate that depends on the position of the interference with respect to the boresight of the antenna and on the ratio $|C/A|$, that is, on the choice of the codes. For limiting this negative effect, the code should be chosen such that $|C/A|<1$, that is the codes used by the two radars should be almost orthogonal. This is not always an easy task. Generally the code is designed for optimizing the frequency and range resolutions of the radar, that is, for optimally shaping the AAF. But often the best-shaped auto-ambiguity corresponds to a very poor CAF, that is, in our problem, high value of $|C/A|$. Some asymptotic bounds on CAF of different classes of frequency hop-coded signals have been reported in [3,13–15]. For Welch–Costas code of length N the bound is N/N then $|C/A|$ can easily get the unit value. For codes based upon linear congruences the bound is $2/N$, then the maximum value of $|C/A|$ is 0.5. Good results can be obtained with a set of the codes based upon extended quadratic congruences for which the asymptotic bound seems to be $12/N$. The adaptive use of different transmitted waveforms to alleviate the impact of an interference is now under analysis [16].

Appendix A. CRLB derivation for deterministic amplitudes

First, let us define some useful vectors and matrices

$$\dot{\mathbf{g}}(\theta)=\frac{\partial \mathbf{g}(\theta)}{\partial\theta},\quad \dot{\mathbf{h}}(\theta)=\frac{\partial \mathbf{h}(\theta)}{\partial\theta} \tag{A.1}$$

and

$$\mathbf{G}(\theta)=\mathbf{g}(\theta)\mathbf{g}^{H}(\theta)=\mathbf{g}(\theta)\mathbf{g}^{T}(\theta),\quad \mathbf{H}(\theta)=\mathbf{h}(\theta)\mathbf{h}^{H}(\theta)=\mathbf{h}(\theta)\mathbf{h}^{T}(\theta), \tag{A.2}$$

$$\dot{\mathbf{G}}(\theta)=\frac{\partial \mathbf{G}(\theta)}{\partial\theta},\quad \dot{\mathbf{H}}(\theta)=\frac{\partial \mathbf{H}(\theta)}{\partial\theta}, \tag{A.3}$$

where the n,mth element of the matrix is $[\dot{\mathbf{G}}(\theta)]_{n,m}=[\dot{\mathbf{g}}(\theta)]_n[\mathbf{g}(\theta)]_m+[\mathbf{g}(\theta)]_n[\dot{\mathbf{g}}(\theta)]_m$, and $[\dot{\mathbf{H}}(\theta)]_{n,m}=[\dot{\mathbf{h}}(\theta)]_n[\mathbf{h}(\theta)]_m+[\mathbf{h}(\theta)]_n[\dot{\mathbf{h}}(\theta)]_m$.

In the case of deterministic amplitudes Eq. (12) reduces to

$$[\mathbf{J}(\boldsymbol{\chi})]_{i,j}=\frac{2}{\sigma_d^2}\Re e\left\{\frac{\partial \boldsymbol{\mu}_y^H(\boldsymbol{\chi})}{\partial\chi_i}\frac{\partial \boldsymbol{\mu}_y(\boldsymbol{\chi})}{\partial\chi_j}\right\},\quad i,j=1,2,\ldots 6. \tag{A.4}$$

Knowing that $\boldsymbol{\mu}_y=ae^{j\varphi}A\cdot\mathbf{g}(\theta_T)+be^{j\psi}C\cdot\mathbf{h}(\theta_I)$, we can calculate

$$\frac{\partial \boldsymbol{\mu}_y(\boldsymbol{\chi})}{\partial\boldsymbol{\chi}}=\begin{bmatrix} ae^{j\varphi}A\dot{\mathbf{g}}(\theta_T)\\ e^{j\varphi}A\mathbf{g}(\theta_T)\\ jae^{j\varphi}A\mathbf{g}(\theta_T)\\ be^{j\psi}C\dot{\mathbf{h}}(\theta_I)\\ e^{j\psi}C\mathbf{h}(\theta_I)\\ jbe^{j\psi}C\mathbf{h}(\theta_I)\end{bmatrix}. \tag{A.5}$$

Setting now $\gamma=|C/A|$, $A=|A|e^{j\vartheta_A}$ and $C=|C|e^{j\vartheta_C}=\gamma|A|e^{j\vartheta_C}$, we obtain for the Fisher matrix elements

$$J_{11}=\frac{2}{\sigma_d^2}a^2|A|^2||\dot{\mathbf{g}}(\theta_T)||^2, \tag{A.6}$$

$$J_{12}=J_{21}=\frac{2}{\sigma_d^2}a|A|^2\dot{\mathbf{g}}^T(\theta_T)\mathbf{g}(\theta_T), \tag{A.7}$$

$$J_{13}=J_{31}=0, \tag{A.8}$$

$$J_{14}=J_{41}=\frac{2}{\sigma_d^2}ab\gamma|A|^2\cos(\vartheta_C-\vartheta_A+\psi-\varphi)\dot{\mathbf{g}}^T(\theta_T)\dot{\mathbf{h}}(\theta_I), \tag{A.9}$$

$$J_{15}=J_{51}=\frac{2}{\sigma_d^2}a\gamma|A|^2\cos(\vartheta_C-\vartheta_A+\psi-\varphi)\dot{\mathbf{g}}^T(\theta_T)\mathbf{h}(\theta_I), \tag{A.10}$$

$$J_{16}=J_{61}=-\frac{2}{\sigma_d^2}ab\gamma|A|^2\sin(\vartheta_C-\vartheta_A+\psi-\varphi)\dot{\mathbf{g}}^T(\theta_T)\mathbf{h}(\theta_I), \tag{A.11}$$

$$J_{22}=\frac{2}{\sigma_d^2}|A|^2||\mathbf{g}(\theta_T)||^2, \tag{A.12}$$

$$J_{23}=J_{32}=0, \tag{A.13}$$

$$J_{24}=J_{42}=\frac{2}{\sigma_{\mathrm{d}}^2}b\gamma|A|^2\ \cos(\vartheta_C-\vartheta_A+\psi-\varphi)\mathbf{g}^{\mathrm{T}}(\theta_{\mathrm{T}})\dot{\mathbf{h}}(\theta_{\mathrm{I}}), \tag{A.14}$$

$$J_{25}=J_{52}=\frac{2}{\sigma_{\mathrm{d}}^2}\gamma|A|^2\ \cos(\vartheta_C-\vartheta_A+\psi-\varphi)\mathbf{g}^{\mathrm{T}}(\theta_{\mathrm{T}})\mathbf{h}(\theta_{\mathrm{I}}), \tag{A.15}$$

$$J_{26}=J_{62}=-\frac{2}{\sigma_{\mathrm{d}}^2}b\gamma|A|^2\ \sin(\vartheta_C-\vartheta_A+\psi-\varphi)\mathbf{g}^{\mathrm{T}}(\theta_{\mathrm{T}})\mathbf{h}(\theta_{\mathrm{I}}), \tag{A.16}$$

$$J_{33}=\frac{2}{\sigma_{\mathrm{d}}^2}a^2|A|^2||\mathbf{g}(\theta_{\mathrm{T}})||^2, \tag{A.17}$$

$$J_{34}=J_{43}=\frac{2}{\sigma_{\mathrm{d}}^2}\mathrm{ab}\gamma|A|^2\ \sin(\vartheta_C-\vartheta_A+\psi-\varphi)\mathbf{g}^{\mathrm{T}}(\theta_{\mathrm{T}})\dot{\mathbf{h}}(\theta_{\mathrm{I}}), \tag{A.18}$$

$$J_{35}=J_{53}=\frac{2}{\sigma_{\mathrm{d}}^2}a\gamma|A|^2\ \sin(\vartheta_C-\vartheta_A+\psi-\varphi)\mathbf{g}^{\mathrm{T}}(\theta_{\mathrm{T}})\mathbf{h}(\theta_{\mathrm{I}}), \tag{A.19}$$

$$J_{36}=J_{63}=\frac{2}{\sigma_{\mathrm{d}}^2}ab\gamma|A|^2\ \cos(\vartheta_C-\vartheta_A+\psi-\varphi)\mathbf{g}^{\mathrm{T}}(\theta_{\mathrm{T}})\mathbf{h}(\theta_{\mathrm{I}}), \tag{A.20}$$

$$J_{44}=\frac{2}{\sigma_{\mathrm{d}}^2}b^2\gamma^2|A|^2||\dot{\mathbf{h}}(\theta_{\mathrm{I}})||^2, \tag{A.21}$$

$$J_{45}=J_{54}=\frac{2}{\sigma_{\mathrm{d}}^2}b\gamma^2|A|^2\dot{\mathbf{h}}^{\mathrm{T}}(\theta_I)\mathbf{h}(\theta_{\mathrm{I}}), \tag{A.22}$$

$$J_{46}=J_{64}=0, \tag{A.23}$$

$$J_{55}=\frac{2}{\sigma_{\mathrm{d}}^2}\gamma^2|A|^2||\mathbf{h}(\theta_{\mathrm{I}})||^2, \tag{A.24}$$

$$J_{56}=J_{65}=0, \tag{A.25}$$

$$J_{66}=\frac{2}{\sigma_{\mathrm{d}}^2}b^2\gamma^2|A|^2||\mathbf{h}(\vartheta_{\mathrm{I}})||^2. \tag{A.26}$$

Based on Eqs. (A.6)–(A.26), we can observe that the Fisher matrix can be written as

$$\mathbf{J}=\begin{bmatrix}\mathbf{A} & \gamma\mathbf{B}\\ \gamma\mathbf{B}^{\mathrm{T}} & \gamma^2\mathbf{C}\end{bmatrix}, \tag{A.27}$$

where **A**, **B** and **C** are three-dimensional sub-matrices. Then, the inverse of **J** can be expressed as

$$\mathbf{J}^{-1}=\begin{bmatrix}\mathbf{D} & \mathbf{E}\\ \mathbf{F} & \mathbf{G}\end{bmatrix}=\begin{bmatrix}(\mathbf{A}-\mathbf{B}\mathbf{C}^{-1}\mathbf{B}^{\mathrm{T}})^{-1} & -\frac{1}{\gamma}(\mathbf{A}-\mathbf{B}\mathbf{C}^{-1}\mathbf{B}^{\mathrm{T}})^{-1}\mathbf{B}\mathbf{C}^{-1}\\ -\frac{1}{\gamma}(\mathbf{C}-\mathbf{B}^{\mathrm{T}}\mathbf{A}^{-1}\mathbf{B})^{-1}\mathbf{B}\mathbf{A}^{-1} & \frac{1}{\gamma^2}(\mathbf{C}-\mathbf{B}^{\mathrm{T}}\mathbf{A}^{-1}\mathbf{B})^{-1}\end{bmatrix}. \tag{A.28}$$

It is worth noting that the sub-matrix **D** does not depend on γ, then the CRLB of θ_{T}, a, and φ do not depend on γ. Conversely, the bounds of the interference parameters are inversely proportional to γ^2.

If the interference is not present, the CRLB of θ_{T}, a, and φ can be calculated simply inverting the matrix **A**. After some algebra we get

$$\mathrm{CRLB}(\theta_{\mathrm{T}})=[\mathbf{J}^{-1}]_{1,1}=\frac{1}{2\mathrm{SNR}}\frac{||\mathbf{g}(\theta_{\mathrm{T}})||^2}{||\dot{\mathbf{g}}(\theta_{\mathrm{T}})||^2||\mathbf{g}(\theta_{\mathrm{T}})||^2-\dot{\mathbf{g}}^{\mathrm{T}}(\theta_{\mathrm{T}})\mathbf{g}(\theta_{\mathrm{T}})\mathbf{g}^{\mathrm{T}}(\theta_{\mathrm{T}})\dot{\mathbf{g}}(\theta_{\mathrm{T}})}. \tag{A.29}$$

Appendix B. CRLB derivation for complex Gaussian distributed amplitudes

In this case, supposing $\alpha\in CN(0,{\sigma_\alpha}^2)$ and $\beta\in CN(0,{\sigma_\beta}^2)$, the observed vector is still Gaussian with a mean value $\boldsymbol{\mu}_y=E\{\mathbf{y}\}=0$ and a covariance matrix $\mathbf{C}_y={\sigma_\alpha}^2|A|^2\mathbf{G}(\theta_{\mathrm{T}})+{\sigma_\beta}^2|C|^2\mathbf{H}(\theta_I)+\sigma_{\mathrm{d}}^2\mathbf{I}$. The unknown parameter vector is $\chi=[\theta_{\mathrm{T}}\quad\theta_I]^{\mathrm{T}}$ and (12) reduces to

$$[\mathbf{J}(\boldsymbol{\chi})]_{i,j}=\mathrm{Tr}\left\{\mathbf{C}_y^{-1}(\boldsymbol{\chi})\frac{\partial\mathbf{C}_y(\boldsymbol{\chi})}{\partial\chi_i}\mathbf{C}_y^{-1}(\boldsymbol{\chi})\frac{\partial\mathbf{C}_y(\boldsymbol{\chi})}{\partial\chi_j}\right\},\quad i,j=1,2. \tag{B.1}$$

It is easy to verify that

$$\frac{\partial\mathbf{C}_y}{\partial\chi_1}=\frac{\partial\mathbf{C}_y}{\partial\theta_{\mathrm{T}}}={\sigma_\alpha}^2|A|^2\dot{\mathbf{G}}(\theta_{\mathrm{T}})$$

and

$$\frac{\partial\mathbf{C}_y}{\partial\chi_2}=\frac{\partial\mathbf{C}_y}{\partial\theta_I}={\sigma_\beta}^2|C|^2\dot{\mathbf{H}}(\theta_{\mathrm{I}}). \tag{B.2}$$

Replacing (B.2) in (B.1) and inverting the Fisher matrix we can obtain the CRLB.

If the interference is not present, the Cramér-Rao bound of θ_{T}, can be easily calculated inverting $[\mathbf{J}]_{1,1}$. After some algebra

$$\mathrm{CRLB}(\theta_{\mathrm{T}})=\frac{1}{\mathrm{SNR}}\frac{1}{\mathrm{Tr}\{[(\mathbf{I}-(\mathrm{SNR}\cdot\mathbf{G}(\theta_{\mathrm{T}})/1+\mathrm{SNR}\cdot\mathbf{g}^{\mathrm{T}}(\theta_{\mathrm{T}})\mathbf{g}(\theta_{\mathrm{T}})))\cdot\dot{\mathbf{G}}(\vartheta_{\mathrm{T}})]^2\}}. \tag{B.3}$$

References

[1] S. Suvorova, D. Musicki, B. Moran, S. Howard, B. La Scala, Multi step ahead beam and waveform scheduling for tracking of manoeuvring targets in clutter, ICASSP05, Philadelphia, USA, March 2005.

[2] S.W. Golomb, H. Taylor, Constructions and properties for Costas arrays, Proc. IEEE 72 (9) (September 1984) 1143–1163.

[3] E.L. Titlebaum, Time–frequency hop signals Part I: coding based upon the theory of linear congruences, IEEE Trans. Aerosp. Electron. Syst. 17 (4) (July 1981) 490–493.

[4] J.R. Bellegarda, E.L. Titlebaum, Time–frequency hop codes based upon extended quadratic congruences, IEEE Trans. Aerosp. Electron. Syst. 24 (6) (November 1988) 726–742.

[5] N. Levanon, E. Mozeson, Radar Signals, IEEE Press, Wiley-Interscience, New Jersey, USA, 2004.

[6] M. Greco, F. Gini, A. Farina, Joint use of $\sum$ and Δ channels for multiple radar target DOA estimation, IEEE Trans. Aerosp. Electron. Syst., in press.

[7] F. Gini, M. Greco, A. Farina, Multiple radar targets estimation by exploiting induced amplitude modulation, IEEE Trans. Aerosp. Electron. Syst. 39 (4) (October 2003) 1316–1321.

[8] S. Kay, Fundamentals of Statistical Signal Processing: Estimation Theory, Prentice-Hall International, Inc., New Jersey, 1993.
[9] W.D. Blair, M. Brandt-Pearce, Monopulse DOA estimation of two unresolved Rayleigh targets, IEEE Trans. Aerosp. Electron. Syst. 37 (2) (April 2001) 452–468.
[10] A.D. Seifer, Monopulse-radar angle measurement in noise, IEEE Trans. Aerosp. Electron. Syst. 30 (3) (July 1994) 950–957.
[11] S.M. Sherman, Monopulse Principles and Techniques, Artech House, Dedham, MA, 1984.
[12] K.-B. Yu, D.J. Murrow, Adaptive digital beamforming for angle estimation in jamming, IEEE Trans. Aerosp. Electron. Syst. 37 (2) (April 2001) 508–523.
[13] S. Maric, I. Seskar, E.L. Titlebaum, On cross-ambiguity properties of Welch-Costas arrays, IEEE Trans. Aerosp. Electron. Syst. 30 (4) (October 1994) 1063–1070.
[14] E.L. Titlebaum, L.H. Sibul, Time–frequency hop signals Part II: coding based upon quadratic congruences, IEEE Trans. Aerosp. Electron. Syst. 17 (4) (July 1981) 494–500.
[15] Y.X. Yang, X.X. Niu, Periodic ambiguity functions of EQC-based TFHC, IEEE Trans. Aerosp. Electron. Syst. 34 (1) (January 1998) 194–199.
[16] M. Greco, F. Gini, P. Stinco, A. Farina, L. Verrazzani, Adaptive Waveform Diversity for Cross-Channel Interference Mitigation, RadarCon2008, Rome, Italy, May 2008.